

Stress tensor changes related to fluid injection at The Geysers geothermal field, California

Patricia Martínez-Garzón,¹ Marco Bohnhoff,^{1,2} Grzegorz Kwiatek,¹ and Georg Dresen¹

Received 25 March 2013; revised 25 March 2013; accepted 29 March 2013; published 7 June 2013.

[1] Studying variations of the stress field in reservoirs caused by massive fluid injection is important toward an improved understanding of geomechanical processes involved. We report on spatio-temporal variations of the local stress tensor orientation at The Geysers geothermal field, California. We apply two stress inversion methods with detailed uncertainty assessments using a selection of events recorded between 2007 and 2012. Our results clearly indicate variations in the orientation of the principal stress axes for the reservoir as a whole showing a normal faulting regime at the reservoir depth between 2 and 3.7 km bounded by a strike-slip regime above and below. Analyzing the temporal evolution of the stress tensor orientation for a prominent seismicity cluster we observe a clear correlation of changes in orientation for σ_{1-3} with the highest injection rates. These results suggest that temporal changes in the stress tensor orientation could contribute to characterize reservoirs during stimulation.

Citation: Martínez-Garzón, P., M. Bohnhoff, G. Kwiatek, and G. Dresen (2013), Stress tensor changes related to fluid injection at The Geysers geothermal field, California, *Geophys. Res. Lett.*, *40*, 2596–2601, doi:10.1002/grl.50438.

1. Introduction

[2] Determining and studying crustal stress field orientations by inverting earthquake focal mechanisms has proven to be a robust and effective tool to study fault mechanics along plate boundaries [e.g., *Hardebeck and Hauksson*, 2001; *Townend and Zoback*, 2001] or even spatiotemporal rotations of principal stresses related to major earthquakes [e.g., *Michael*, 1987a; *Bohnhoff et al.*, 2006]. While stress rotations in most studies were in the order of 10–20° at best and thus close to the typical resolution limit of most data sets, recent $M \sim 9$ megathrust earthquakes showed larger stress rotations ($>20^\circ$) clearly associated with the mainshock ruptures [*Hasegawa et al.*, 2011; *Hardebeck*, 2012].

[3] Stress inversion techniques have also been applied to induced seismicity related to fluid injection into different types of reservoirs [*Oppenheimer*, 1986; *Feng and Lees*, 1998; *Sasaki and Kaieda*, 2002; *Bohnhoff et al.*, 2004].

These studies have mainly focused on spatial analyses around the geothermal area and particularly on the variations in stress field orientation with depth.

[4] Spatio-temporal variations of the crustal stresses on the reservoir scale may be caused by massive fluid injections and extractions [*Segall and Fitzgerald*, 1998]. Detection of potential stress changes is important toward an improved understanding of the associated geomechanical processes at reservoir depth. However, an accurate and reliable determination of injection-induced changes in stress orientation is not trivial and requires dense local seismic networks allowing determining reliable and accurate focal mechanism data. For this reason, such observations are still few and a description of the stress field response of a reservoir where massive fluid injection is performed remains not fully understood.

[5] In this study, we investigate potential spatial and temporal variations of the stress field orientation at The Geysers (TG) geothermal area, which provides the largest existing data set of induced seismicity with $\sim 500,000$ events since the beginning of operation in the 1960s. We also selected this data set due to the great amount of local and regional seismic networks and stations available allowing calculating reliable focal mechanisms. First, we calculate the stress tensor orientation at different depths (local coordinate system) throughout TG. Second, we investigate a prominent cluster of induced seismicity within the reservoir and relate the stress inversion results to injection rates of the two nearby wells. Our main goal is to determine whether changes in the stress field can contribute to detect (or even monitor) potential changes in a reservoir due to fluid injection.

2. Data and Method

[6] We used the stress inversion software package SATSI developed by *Hardebeck and Michael* [2006]. SATSI is a linearized inversion scheme which uses focal mechanisms (strike/dip direction/dip angle) as input data. It allows for a spatial and/or temporal subdivision of the focal mechanism data set into smaller subareas. Then, a damped inversion method is applied to resolve the stress field orientation for each subarea taking into account the adjacent subareas to smooth the solution. Therefore, only strong heterogeneities of the stress tensor are left, while other variations, e.g., artifacts arising from data subdivision are smoothed. When using SATSI, we selected only seismic events with more than 10 high-quality first-motion polarities available (weight 0 as defined in *Klein* [2006]). Complementary, we also applied the MOTSI stress inversion method [*Abers and Gephart*, 2001]. MOTSI is a nonlinear scheme using first motion polarities as input data. Here, two nested grid searches are performed to identify the best-fitting stress orientations and focal mechanisms. The outer search tries a

¹Section 3.2 Geomechanics and Rheology, GFZ German Research for Geosciences, Telegrafenberg, 14473 Potsdam, Germany.

²Free University Berlin, Institute of Geological Sciences, Berlin, Germany.

Corresponding author: P. Martínez-Garzón, Section 3.2 Geomechanics and Rheology, GFZ German Research for Geosciences, Telegrafenberg, 14473 Potsdam, Germany. (patricia@gfz-potsdam.de)

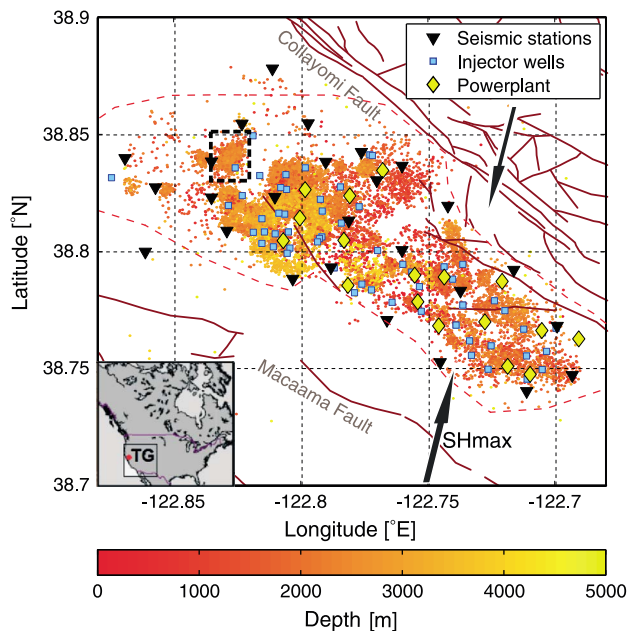


Figure 1. Spatial distribution of seismic events at The Geysers ($M > 1$) from September 2007 to July 2012 (Data from NCEDC catalog). Hypocentral depth is color encoded. Selected cluster for temporal stress field variation analysis is surrounded with a black rectangle. Black triangles represent the local seismic network from LBNL. Yellow rhombs represent active powerplants, blue squares represent injection wells (not all wells from the field are plotted). Black arrows represent the direction of the regional stress field as described in *Oppenheimer* [1986] and *Provost and Houston* [2003]. Bottom-left corner: Overview on the location of TG in North America.

range of values for three stress directions and a relative stress magnitude $R = (\sigma_1 - \sigma_2) / (\sigma_1 - \sigma_3)$. Then, an inner grid search is conducted for each stress model and determines the focal mechanisms that best fit the first motions. To perform stress inversion with MOTSI we selected only events with a minimum of 20 high-quality first-motion polarities available (as recommended by *Abers and Gephart* [2001] to ensure correct results with this method). Outputs of both methods are the orientations of the principal stresses, σ_1 , σ_2 , σ_3 , and a relative stress magnitude.

[7] To investigate the local stress tensor at TG we selected the hypocenter catalogue, fault plane solutions and first motion polarities as provided by Northern California Earthquake Data Center (NCEDC). We focus our study on the time period September 2007 to June 2012. The analyzed data set contained approx. 16,800 seismic events that occurred within TG area (Figure 1). They were recorded by a local seismic network operated by Lawrence Berkeley National Laboratory (LBNL), and by several regional permanent stations deployed at different distances around TG. The hypocenters were determined with the absolute location method HYPOINVERSE [*Klein*, 2002]. The local multilayered 1-D velocity model provided by *Eberhart-Phillips and Oppenheimer* [1984] is considered. Given the reasonably good azimuthal coverage of the seismic events and the large number of stations, the reported average horizontal location error for the NCEDC catalog calculated with HYPOINVERSE is 200 m and the vertical location error is 300 m.

[8] In a first step we searched for potential depth-dependent variations of the stress field orientation (Figure 2). For this part we selected seismic events with their epicenters distributed over the whole reservoir and sorted them according to the increasing depth. We performed a stress inversion of focal mechanisms using SATSI and a subset of first (shallowest) 150 events. Then, we moved by 100 events and repeated the inversion again using 150 events (i.e., the second subset contained 50 events overlapping with first one). This procedure (moving-depth window) was repeated until the last possible depth subset (containing the deepest 150 events). A few selected depth subsets are shown in Figures 2b and 2c, together with the corresponding results of stress inversion (Figure 2a). For comparison we also performed separate stress inversions using MOTSI.

[9] For the temporal analysis, we selected seismic data from a spatially constrained seismicity cluster located in the northwestern part of the reservoir (rectangle in Figure 1). In the direct vicinity of the cluster there are two wells for fluid injecting. The first well is used as a demonstration site for an Enhanced Geothermal System; there, injection resumed in November 2007. At the second well, injections started on April 2010. Gross amount of fluid injected is remarkably lower than in the first well, although both follow the same seasonal tendency (gross amount of fluid injected during winter months is higher than in summer months). During these injections, 742 earthquakes occurred. Their magnitudes vary between 1.0 and 3.1, and the majority of them are located at depths between 2000 and 3000 m. There is no first-order depth variation throughout the analyzed interval. If more than one possible focal mechanism was provided, we selected the one with the smallest misfit. The focal mechanism catalog includes a substantial variation in mechanisms allowing for a reliable estimation of stress field orientation. Sorting the events with time we formed subsets of 55 events and inverted moving windows with 10-event increments using the SATSI stress inversion. The number of events in one subset was selected to balance a tradeoff between the discrimination of different injection stages and the insurability of a certain variety of focal mechanisms. The required variety of focal mechanisms for each stress inversion was checked by inspection of the respective distribution of P and T axes.

[10] Because we aimed at detecting relatively small variations in the stress field orientation that could be close to the resolution limit of the methods applied, we performed complete uncertainty assessments for both used inversion methods. For SATSI we used bootstrap resampling method. Each fault plane solution taken into inversion was selected randomly from the two nodal planes available (i.e., we do not have a preference for one of the two permitted fault planes). For MOTSI the uncertainties were estimated applying a Bayesian technique. All inversion results shown in the following sections provide the best solution as well as the 95% confidence interval (2σ).

3. Results

3.1. Depth-Dependent Stress Field Changes

[11] Inverting subsets formed after hypocentral depth with the SATSI routine we find clear changes of the stress field orientation with depth (Figure 2a). At shallower level (down to $Z = 1000$ m) the σ_1 and σ_3 axes are oriented subhorizontal

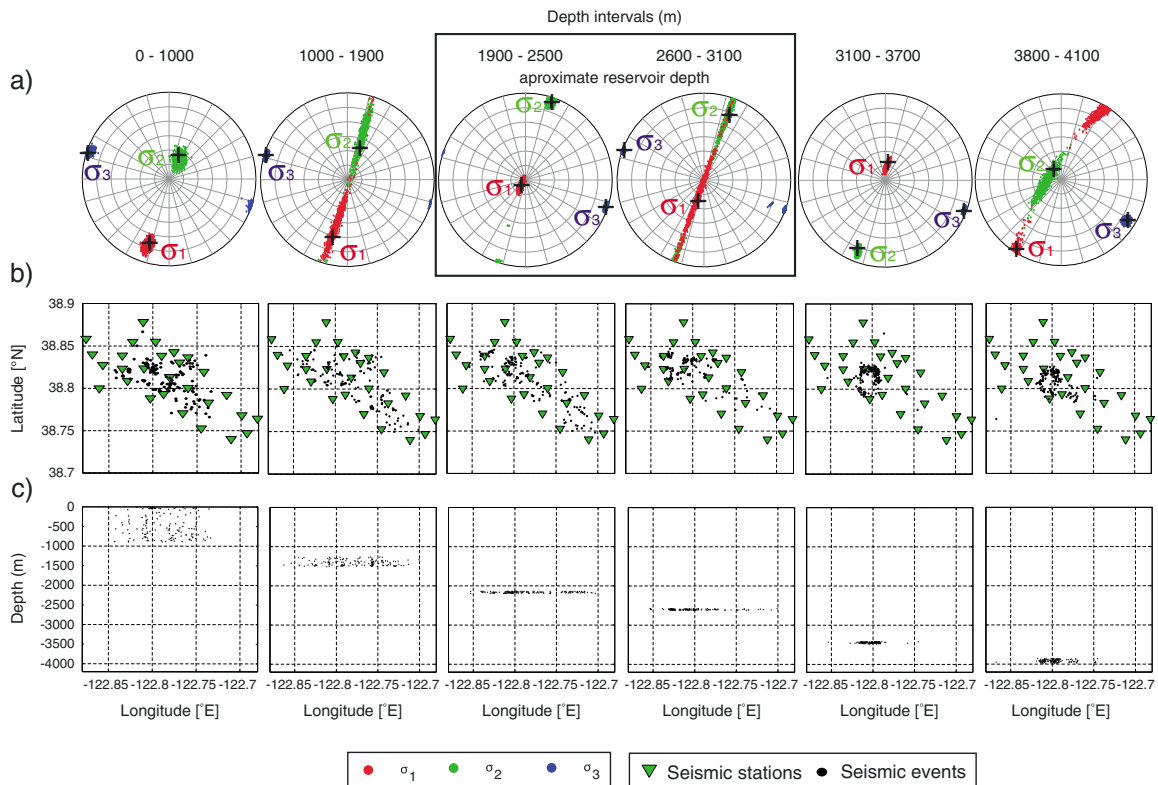


Figure 2. (a) Example of stress inversion results (lower hemisphere projection) representative for the average stress orientation of the total of inversions performed in each depth interval (depths in local coordinate system). Red, green and blue colors correspond to σ_1 , σ_2 , and σ_3 axes, respectively. Dots represent sampled bootstrap points framing the 95% confidence intervals. Black crosses mark the best stress orientation obtained from inversion. (b) Epicentral distribution of seismicity used in the corresponding inversion shown in Figure 2a. Green triangles represent seismic network from LBNL. (c) Seismic events from Figure 2b represented as a function of depth (note that as described in the text, several other stress inversions are performed, and therefore the seismic events plotted here are not representative of the total amount of seismicity but just for those event used in one particular inversion).

corresponding to a strike-slip regime. Between $Z=1000$ m and $Z=1900$ m, the position of the σ_1 and σ_2 axes is undefined considering plunges, indicating a transtensional stress regime. Between $Z=1900$ m and $Z=2500$ m, the σ_1 and σ_2 axes stabilize and σ_1 becomes vertical indicating a WSW/ENE-extensional normal faulting regime. Further below and down to $Z=3800$ m changes to transtensional and normal faulting are repeated. Finally, at the deepest analyzed intervals $Z=3800$ m to $Z=4100$ m (below the geothermal reservoir) the σ_1 axis rotates back toward subhorizontal suggesting a strike-slip/transtensional regime as observed above the reservoir. As shown in Figures 2b and 2c for six selected depth intervals, the epicentral distribution of the seismic events considered for stress inversion is approximately homogeneous throughout the reservoir down to $Z=2600$ m, while below this depth the hypocenters cluster in the central part of the reservoir delineating a circular structure [Boyle *et al.*, 2011]. The deepest seismicity is observed in the central and western part of the reservoir (cf. two right-most depth intervals presented in Figure 2). In all performed stress inversions the σ_3 axis is located subhorizontal pointing to $N105^\circ E$. The trend of σ_1 and σ_2 remains stable at $N15^\circ E$. Only for the deepest part of the reservoir the trend of σ_1 and σ_2 seems to be slightly rotated clockwise by 15° .

[12] The results from MOTSI generally follow those from SATSI described before with σ_1 and σ_3 being

subhorizontally oriented in the shallower section. In contrast, the result for the deeper section includes a substantially steeper direction for σ_1 reflecting a strong normal faulting component. However, because the confidence intervals for σ_1 and σ_2 are partly overlapping the results indicate a transtensional stress regime at larger depth. This is also confirmed by the low values for the relative stress magnitude R obtained from both inversion routines.

3.2. Time-Dependent Stress Field Changes

[13] Analyzing the distribution of P and T axes of the 742 seismic events from the selected cluster suggests systematic variations during the investigated 5 year time period that can be easily correlated to injection rates (Figure 3a). The plunges of P axes before and after time periods with maximum injection rates are mainly distributed around the vertical direction. Remarkably, during the times of maximum flow rates P axes plunges decrease. We selected two time intervals framing the most prominent three peak injections (Intervals A and B, see black rectangles in Figure 3b) and performed a detailed time-dependent stress inversion analysis as described above using subsets of the data. The results confirm a clear and statistically significant relation between injection rates and changes in stress field orientation for all three principal stress axes (Figure 3c).

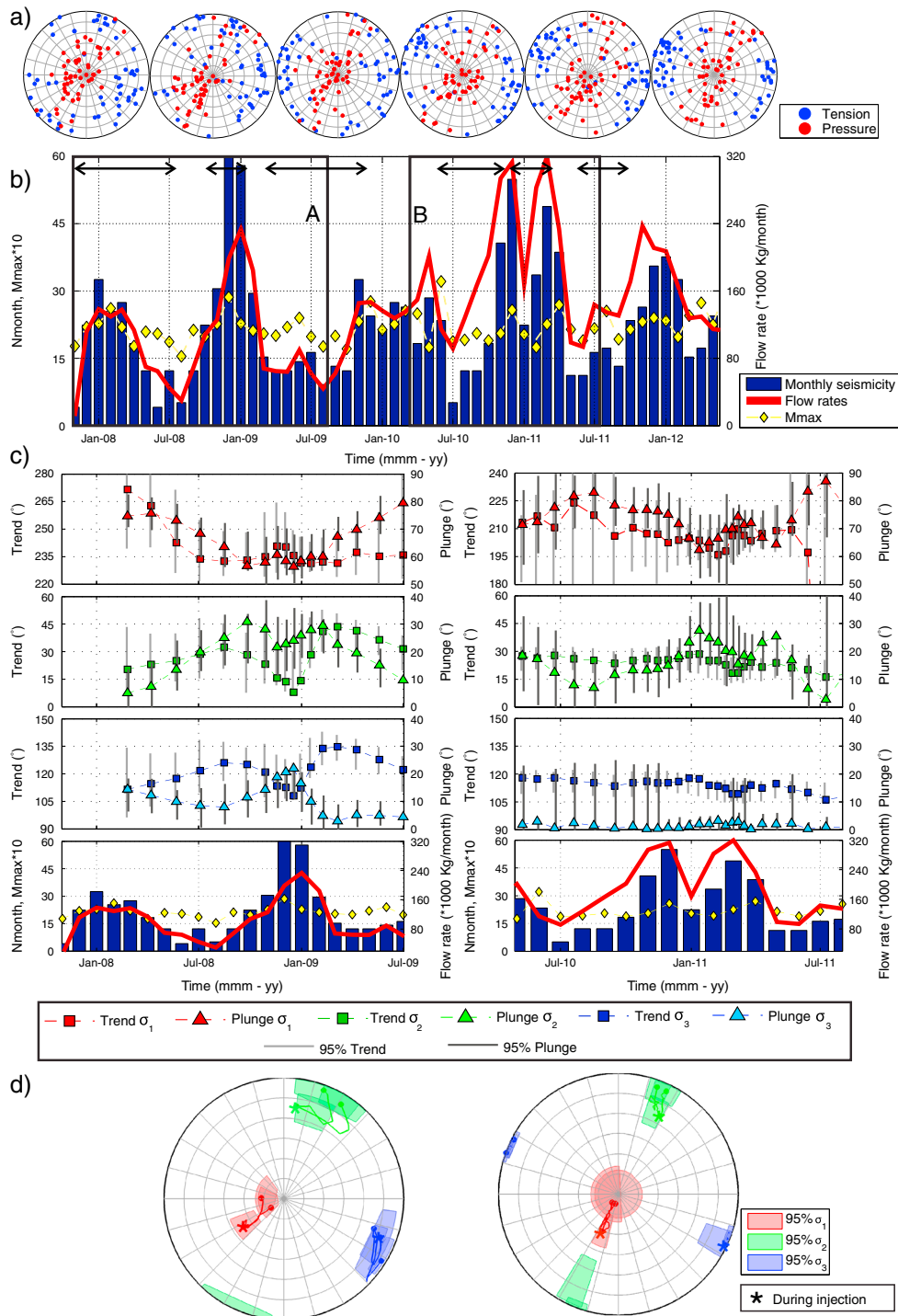


Figure 3. (a) Distribution of P and T axes of events used for stress inversions which contain seismic events from before, during and after the analyzed injections, respectively. The time frame covered in each plot is shown with the consecutive black horizontal arrows in Figure 3b. (b) Monthly seismicity rate from events from analyzed cluster (blue bars) from November 2007 to July 2012. Injection rates (gross amount injected/month) are plotted as a sum from both considered wells (solid red line). The maximum magnitude of each month is shown by a yellow rhomb. The black rectangles frame the two analyzed time intervals (A and B). (c) Results from the stress inversions performed during the time interval framed by black rectangles in Figure 3b. Each symbol represents one stress inversions which time average corresponds to the X coordinate. From top to bottom: Trend (squares) and plunge (triangles) of σ_1 (first plot – red), σ_2 (second plot – green) and σ_3 (third plot – blue). For these three graphics, light and dark gray vertical bars represent 95% confidence intervals of trend and plunge, respectively. Next plot contains a zoom from b) corresponding to the analyzed time intervals. (d) Variations of the stress field orientation during the selected time frames plotted in the lower hemisphere. Red: σ_1 , Green: σ_2 , Blue: σ_3 . Solid lines: Trajectory described by the best solution. Semitransparent region: 95% confidence interval corresponding to three inversions before, during and after the performed inversions.

[14] The change in plunge of σ_1 is similar for all three injections. Prior to an injection, the σ_1 axis is close to vertical. Inversion of faulting mechanisms from seismic events that occurred during peak-injection rates results in a progressive decrease in the plunge of σ_1 . Moreover, including seismic events from the time period after the injection peak, the σ_1 axis rotates back toward close to its initial vertical position. The change in the plunge of σ_1 is significant and varies between 15° and 20° .

[15] During interval A (peak-injection in December 2008), the plunges of the σ_2 and σ_3 axes also vary in accordance with injection rates. The plunge of σ_2 increases gradually and then during injection it slightly decreases by 15° . Similarly, the plunge of σ_3 gradually increases until the peak-injection and then decreases toward values from prior to the injection. For both σ_2 and σ_3 axes a counterclockwise and transient change in the axes trend is observed by about 25° . During interval B (peak injections in December 2010 and March 2011) the plunges of σ_1 and σ_2 show the most pronounced correlation with the gross amount of fluid injected. They show an inverse variation of approximately 20° . The plunge of σ_3 remains constant.

[16] There are two minor but important differences between the two analyzed periods: First, the time interval A shows variations in both trend and plunge of the three principal axes, while for the interval B no remarkable changes in trend are observed but the plunge of the σ_1 and σ_2 axes varies significantly. Second, during interval A the change in stress orientation is synchronous with fluid injection, whereas in interval B the stress changes appear slightly delayed.

4. Discussion and Conclusions

[17] Due to the high rate of seismicity at The Geysers geothermal field and the exceptionally good quality of the seismic data available, this data set provides a good opportunity to derive a better understanding on the effects of fluid injection on the stress state in the reservoir. In this study, stress inversion methods have been applied to two data subsets of induced seismicity. For the first case, the seismic events are distributed over the entire reservoir and we searched for potential variations of the stress tensor orientation with reservoir depth. For the second case, seismic events from a particular cluster of events were analyzed with regard to potential temporal variations in the orientation of the local stress field related to fluid injection in two wells. In both cases, the variations observed are significant considering 95% of confidence interval.

[18] Studies about the regional stress field of Northern and Central California indicate that the stress field around TG is consistent with a strike-slip regime with the direction of maximum horizontal compression being oriented N26°E, and thus inclined by 55° with respect to the regional strike of the San Andreas Fault system [Provost and Houston, 2003; Hardebeck and Michael, 2004]. No first-order spatial variations within TG have been reported [e.g., K. Boyle and M. Zoback, pers. comm., 2012]. In general, our analysis shows a combined strike-slip/normal faulting regime consistent with the known regional stress field in Northern California.

[19] Results from depth-dependent changes of the stress field orientation indicate a transition in the stress regime from strike slip above the reservoir to transtensional and normal at the reservoir level and finally transtensional and

strike-slip below. This clear variation of the stress field orientation with depth is due to the flip of the plunges of the σ_1 and σ_2 axes, while their trend remains constant at N15°E. The changes observed in these axes are in accordance with changes in the value of the relative stress magnitude R , indicating that the magnitudes of σ_1 and σ_2 are less separated within the reservoir than outside.

[20] The cause of the changes in stress orientations observed with depth across the TG reservoir is still not well understood. A potential explanation could be related to the presence of fluids in the vapor-saturated reservoir level. The role of fluids modifying the stress field and the faulting regime has been already pointed out in earlier studies [e.g., Hardebeck and Hauksson, 1999; Kato et al., 2011]. In particular, Segall and Fitzgerald [1998] related a potential vertical variation of the stress state within the reservoir, above and below it to poroelastic effects related to reservoir depletion, i.e., on a time scale of decades. Specifically, the authors suggest that the horizontal stresses immediately above and below a reservoir are more compressive than within the reservoir. This is in qualitative agreement with the observed change in maximum compressive stress orientation from about horizontal above and below the reservoir to vertical within the reservoir. However, a quantitative assessment of interaction of stress rotation with variations in fluid pressure and depth does not yet exist for TG. Alternatively, the variations of the stress regimes with depth could also be related to the different geological formations within and above/below the reservoir. Particularly, the transition from graywacke sandstone to thermally altered graywacke sandstone where the temperature gradient is extremely high could affect the state of stress in the rocks, while a correlation between the average stress regime and the different geological layers remains imprecise due to the irregular high temperature layer at TG [Calpine Corporation, 2012].

[21] Although one of the assumptions for the inversion of fault plane solutions to determine the stress field orientation is a homogeneous stress field within the volume considered by the individual focal mechanism hypocenters [Michael, 1987b], we believe that the stress field at TG might have local spatial variations due to different injection and production sites and schedules. For this reason, the stress field orientations calculated in this part of the study provides an average of the expected different local stress field orientations throughout TG.

[22] In the second part of the study we analyzed potential temporal variations of the stress field orientation focusing on one particular spatially well-constrained seismicity cluster at the northwest of TG. Our results clearly show a systematic rotation of the principal stress axes during periods of massive fluid injection (Figure 3). This observation for itself is remarkable in that it allows using an observed stress field orientation as a proxy for a change in the geomechanical status of a (geothermal) reservoir, e.g., during stimulation through massive fluid injection. More interestingly, this correlation of stress field rotation and peak-injection rates is observed in all cases analyzed so far. On the other hand, the variation is more evident in the first remarkable injection performed in the investigated area (corresponding to interval A). This observation suggests that the effect of the stress perturbation due to the fluid injection might decrease over time with repeated injections. This might also be seen as an explanation for the delayed stress

change during the second peak-injection period. It is well known that the injection of fluid increases the pore pressure of the rock matrix and according to the rock failure criteria it facilitates the slip of the rocks. However, a complete geomechanical explanation of the stress tensor changes observed in our study leaves open several questions. The existence of local faults at TG NE/SW oriented is consistent with the direction of regional maximum horizontal stress. In response to the three injections considered in our study, the σ_1 axes are moving toward shallower plunges, while the trend is changing by a lesser extent and being in SW direction in first-order approximation. One potential explanation for the observed stress tensor perturbation, therefore, is that with the massive fluid injections, preexisting local faults and fractures well-oriented for the regional stress would be reactivated or weakened for a short interval during high injection rates. A second possibility might be related to the fact that the analyzed cluster of seismicity is the result of one of the few Enhanced Geothermal System project performed at TG involving massive fluid injection and thereby aiming at increasing the permeability of the reservoir. Therefore, the active stimulation of the low-permeable reservoir may imply hydro-fracturing. It is then possible that during the time periods with higher injection rates of cold water, new small fractures were created and might have opened. These small fractures would then be oriented in the direction of σ_{Hmax} (NE-SW) and their activation could also perturb the stress field in the observed way.

[23] **Acknowledgments.** We acknowledge funding within the Helmholtz-Alberta Initiative, from the Helmholtz foundation in the framework of the YIG “From microseismicity to large earthquakes” and from the EU-GEISER project. We acknowledge seismic data availability from North California Earthquake Data Centre and hydraulic parameters from Department of Conservation State of California. We thank Roland Gritto, Calpine Ltd. and Michèle Ickrath. We thank Volker Oye and an anonymous reviewer for their comments.

[24] The Editor thanks Volker Oye and an anonymous reviewer for their assistance in evaluating this paper.

References

- Abers, G. A., and J. W. Gephart (2001), Direct inversion of earthquake first motions for both the stress tensor and focal mechanisms and application to southern California, *J. Geophys. Res.*, *106*, 26,523–26,540, doi:10.1029/2001JB000437.
- Bohnhoff, M., S. Baisch, and H.-P. Harjes (2004), Fault mechanisms of induced seismicity at the super deep German Continental Deep Drilling Program (KTB) borehole and their relation to fault structure and stress field, *J. Geophys. Res.*, *109*, B02309, doi:10.1029/2003JB002528.
- Bohnhoff, M., H. Grosser, and G. Dresen (2006), Strain partitioning and stress rotation at the North Anatolian Fault after the 1999 Izmit $M_w=7.4$ earthquake, *Geophys. J. Int.*, *166*(1), 373–385, doi:10.1111/j.1365-246X.2006.03027.X.
- Boyle, K., S. Jarpe, L. Hutchings, S. Saltiel, J. Peterson, and E. Majer (2011), Preliminary investigation of an aseismic “doughnut hole” region in the northwest Geysers, California, PROCEEDINGS, Thirty-Sixth Workshop on Geothermal Reservoir Engineering Stanford University, Stanford, California, January 31 - February 2, 2011 SGP-TR-191.
- Calpine Corporation (2012), NW Geysers Enhanced Geothermal System Demonstration Project, *Update Report*, http://www.geysers.com/docs/11022012%20EGS_Community%20Update%20Presentation.pdf
- Eberhart – Phillips, D., and D. Oppenheimer (1984), Induced Seismicity in The Geysers Geothermal Area, California, *J. Geophys. Res.*, *89*(B2), 1191–1207.
- Feng, Q., and J. M. Lees (1998), Microseismicity, stress, and fracture in the Coso geothermal field, California, *Tectonophysics*, *289*, 221–238.
- Hardebeck, J. L., and E. Hauksson (1999), Role of Fluids in Faulting Inferred from Stress Field Signatures, *Science*, *285*, 236, doi:10.1126/science.285.5425.236.
- Hardebeck, J. L., and E. Hauksson (2001), Crustal stress field in southern California and its implications for fault mechanics, *J. Geophys. Res.*, *106*, 21,859–21,882.
- Hardebeck, J. L., and A. J. Michael (2006), Damped regional-scale stress inversions: Methodology and examples for Southern California and the Coalinga aftershock sequence, *J. Geophys. Res.*, *111*, B11310, doi:10.1029/2005JB004144.
- Hardebeck, J. L., and A. J. Michael (2004), Stress orientations at intermediate angles to the San Andreas Fault, California, *J. Geophys. Res.*, *109*, B11303, doi:10.1029/2004JB003239.
- Hardebeck, J. (2012), Coseismic and postseismic stress rotation due to great subduction zone earthquakes, *Geophys. Res. Lett.*, *39*, L21313, doi:10.1029/2012GL053438.
- Hasegawa, A., K. Yoshida, and T. Okada (2011), Nearly complete stress drop in the 2011 Mw 9.0 off the Pacific coast of Tohoku earthquake, *Earth Planets Space*, *63*(7), 703–707, doi:10.5047/eps.2011.06.007.
- Kato, A., et al. (2011), Anomalous depth dependency of the stress field in the 2007 NotoHanto, Japan, earthquake: Potential involvement of a deep fluid reservoir, *Geophys. Res. Lett.*, *38*, L06306, doi:10.1029/2010GL046413.
- Klein, F. W. (2002), User’s Guide to HYPOINVERSE-2000, a Fortran Program to Solve for Earthquake Locations and Magnitudes, Open file report. URL: <http://geopubs.wr.usgs.gov/open-file/of02-171/>
- Klein, F. W. (2006), Y2000 shadow format and NCSN data codes. Open file report, URL: <http://www.ncedc.org/ftp/pub/doc/ncsn/shadow2000.pdf>
- Michael, A. J. (1987a), Stress Rotation during the Coalinga Aftershock Sequence, *J. Geophys. Res.*, *92*, 7963–7979.
- Michael, A. J. (1987b), Use of focal mechanisms to determine stress: a control study, *J. Geophys. Res.*, *92*, 357–368.
- Oppenheimer, D. (1986), Extensional tectonics at The Geysers Geothermal Area, California, *J. Geophys. Res.*, *91*, 11,463–11,476.
- Provost, A. S., and H. Houston (2003), Stress orientation in northern and central California: Evidence for the evolution of frictional strength along the San Andreas plate boundary system, *J. Geophys. Res.*, *108*(B3), 2175, doi:10.1029/2001JB001123.
- Sasaki, S., and H. Kaieda (2002), Determination of stress state from local mechanisms of microseismic events induced during hydraulic injection at the Hijiori Hot Dry Rock site, *Pure Appl. Geophys.*, *159*, 489–516.
- Segall, P., and S. D. Fitzgerald (1998), A note on induced stress changes in hydrocarbon and geothermal reservoirs, *Tectonophysics*, *289*, 117–128.
- Townend, J., and M. D. Zoback (2001), Implications of earthquake focal mechanisms for the frictional strength of the San Andreas fault system, *Geol. Soc. Spec. Publ. London*, *186*, 13–21, doi:10.1144/GSL.SP.2001.186.01.02.